Langmuir

ARTICLE

pubs.acs.org/Langmuir

Multicore−Shell PNIPAm-*co*-PEGMa Microcapsules for Cell Encapsulation

Tatiya Trongsatitkul and Bridgette M. Budhlall*

NSF Center for High-Rate Nanomanufacturing and Department of Plastics Engineering, University of Massachusetts, Lowell, Massachusetts 01854, United States

Supporting Information

ABSTRACT: The overall goal of this study was to fabricate multifunctional core−shell microcapsules with biological cells encapsulated within the polymer shell. Biocompatible temperature responsive microcapsules comprised of silicone oil droplets (multicores) and yeast cells embedded in a polymer matrix (shell) were prepared using a novel microarray approach. The cross-linked polymer shell and silicone multicores were formed in situ via photopolymerization of either poly(*N*-isopropylacryamide)(PNIPAm) or PNIPAm, copolymerized with poly(ethylene glycol monomethyl ether monomethacrylate) (PEGMa) within the droplets of an oil-in-water-in-oil double emulsion. An optimized recipe yielded a multicore−shell morphology, which was characterized by optical and laser scanning confocal microscopy (LSCM) and theoretically confirmed by spreading coefficient calculations. Spreading coefficients were calculated from interfacial tension and contact angle measurements as well as from the determination of the Hamaker constants and the pair potential energies. The effects of the presence of PEGMa, its molecular weight (M_n 300 and 1100 g/mol), and concentration (10, 20, and 30 wt %) were also investigated, and they were found not to significantly alter the morphology of the microcapsules. They were found, however, to significantly improve the viability of the yeast cells, which were encapsulated within PNIPAm-based microcapsules by direct incorporation into the monomer solutions, prior to polymerization. Under LSCM, the fluorescence staining for live and dead cells showed a 30% viability of yeast cells entrapped within the PNIPAm matrix after 45 min of photopolymerization, but an improvement to 60% viability in the presence of PEGMa. The thermoresponsive behavior of the microcapsules allows the silicone oil cores to be irreversibly ejected, and so the role of the silicone oil is 2-fold. It facilitates multifunctionality in the microcapsule by first being used as a template to obtain the desired core−shell morphology, and second it can act as an encapsulant for oil-soluble drugs. It was shown that the encapsulated oil droplets were expelled above the volume phase transition temperature of the polymer, while the collapsed microcapsule remained intact. When these microcapsules were reswollen with an aqueous solution, it was observed that the hollow compartments refilled. In principle, these hollow-core microcapsules could then be filled with water-soluble drugs that could be delivered in vivo in response to temperature.

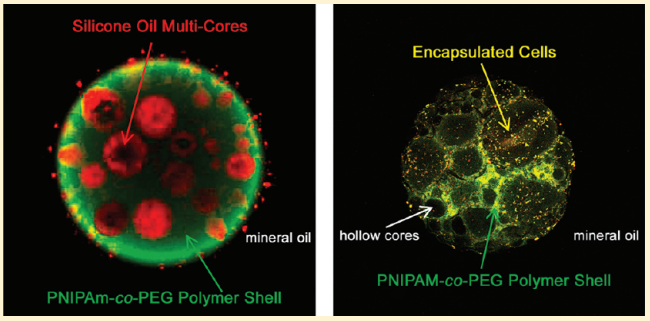

1. INTRODUCTION

Cell microencapsulation has been studied for many decades[1] and can be developed into various applications, such as cell therapy,[2] cell biosensors,[3] and probiotic encapsulation by the food or nutraceutic industries.[4] In cell encapsulation applications, complex and conflicting requirements have to be met. One of the most important considerations for the design of a cell microencapsulation device is material biocompatibility with the encapsulated cells and surrounding host tissue and for the material not to interfere with cell homeostasis. Another important consideration is to employ a gentle encapsulation technique such as using aqueous medium. Reactive species or organic solvents should not be used to preserve cell integrity. Hydrogels have been reported[5] to meet these requirements for cell encapsulation devices.

Hydrogels are three-dimensional networks of hydrophilic polymers, which can absorb water several times greater than their corresponding dry weight. The unique properties of hydrogels that make them a material of choice for biomedical applications include minimal interfacial tension with surrounding biological fluids, permeation, and diffusion of low molecular weight compounds. Hydrogels also match the flexibility of human tissue, due to their water content, which reduces mechanical and frictional irritation to tissues and cells.[6] Hydrogel networks can be designed using cross-linking methods that are conducive with cell viability, usually involving noncovalent cross-linking.[7] Covalently cross-linked hydrogels would have significant advantages in terms of stability; however, toxicity of reactants and the time required to complete chemical cross-linking were reported

Received: August 3, 2011
Revised: September 27, 2011

dx.doi.org/10.1021/la203030j | *Langmuir* XXXX, XXX, 000–000

to be generally incompatible with cell survival. Hydrogel-embedding has several advantages as the cells are kept in an aqueous environment in contact with soft, biocompatible materials, protected from the stress of encapsulation.

For drug delivery applications and cell encapsulation, colloidal hydrogels with two morphologies (microgels and microcapsules) are most often used. These terms are occasionally used interchangeably. A microgel is a cross-linked particle, which is swollen by a good solvent and is normally prepared by emulsion or dispersion polymerization methods. The maximum extent of swelling is controlled by the amount of cross-linking monomer that is copolymerized. Conversely, a microcapsule is a particle with core−shell morphology, where the shell can be a cross-linked polymer with a single or multiple liquid or hollow cores.

Although significant milestones have been attained with microgel-enclosed cell systems, few clinical studies have been reported to date,[8] and the potential for this technique has not been fully realized. Liquid core−shell microcapsules generally seem to allow better cell growth and protein production.[5]

Microcapsules synthesized with a core−shell morphology using thermoresponsive cross-linked poly-*N*-isopropylacrylamide (PNIPAm) as a polymer shell are an attractive structure because of their ability to carry substances within their core for drug delivery and release applications.[9] PNIPAm has also been previously utilized for tissue culture surfaces.[10] Cross-linked PNIPAm is classified as a "smart" polymer due to its responsiveness to external stimuli, specifically temperature.[11−13] As temperature increases, the polymer chain network collapses and separates out of the aqueous solution. This behavior indicates that the polymer becomes less water-soluble upon heating, in contrast with the behavior of most compounds in aqueous solution.[13−17] This phenomenon has been extensively investigated.[14−18] The change in solubility of PNIPAm reflects its macromolecular transition from a hydrophilic to a hydrophobic structure (coil-to-globule transition), which occurs rather abruptly and is known as the lower critical soluble temperature (LCST). For PNIPAm linear homopolymer, the LCST was established to be 32 °C in the aqueous phase.[18−20] When the polymer is cross-linked, a network is formed and responds as a volume collapse arising from the expulsion of water. This transition temperature is referred to as a "volume phase transition temperature" (VPTT), which is close to LCST of the corresponding linear polymer.

Various forms of PNIPAm appear in the literature including single chains, macroscopic gels,[21,22] microgels,[17,23−27] latex,[28] thin films,[29,30] membranes,[31] coating,[32,33] and fibers.[34,35] Early research focused on the theoretical aspects of LSCT, where PNIPAm conformation undergoes the change from a coil-to-globular structure in diluted aqueous solutions,[13−15,36] whereas more recent work has emphasized a wide range of exciting applications. The fact that PNIPAm possesses the most well-defined transition among all thermoresponsive polymers, with a LSCT close to physiological temperature, makes PNIPAm the most extensively and intensively studied hydrogel. The potential applications of this special temperature responsive polymer include chromatography,[37] extraction compounds, surface modifiers, switching devices, sensors, drug delivery, and gene delivery. Recently, self-folding poly(ε-caprolactone) was copolymerized with PNIPAm to form microcapsules. This material was used to reversibly encapsulate and release yeast cells in response to temperature; however, no cell viability studies were performed.[38] It was also shown by Luo and co-workers that yeast cells could be successfully encapsulated into agarose capsules using a microfluidic device.[39] A hydrodynamic flow focusing geometry was used to produce agarose droplets with a cell suspension in the aqueous phase. Again, no release mechanism or cell viability studies were presented.

PNIPAm may be rendered biocompatible for cell and drug delivery applications by covalently attaching polyethylene glycol (PEG) to PNIPAm polymer in a process called PEGylation.[40] PEG is known to be safe and biocompatible. Previous studies have also shown that PEG can render stealth properties to microgels by coating or grafting to the outer surface. This modification facilitates the formation of hydrogen bonds between the oxygen atoms on the PEG segment and water molecules, providing the PEG segments with a protective hydration shell that minimizes nonspecific interactions of the microgels within the biological environment.[23,41] As such, PEG was used in the current study to achieve increased residence life of the microcapsule within the body, thereby improving the local tissue retention of the released payloads (e.g., drugs or cells). PEG may, however, affect the morphology of the microcapsule as it may change the interfacial tension of the system. Therefore, understanding the loci of PEG in our microcapsule is critical to an understanding of the effect of PEG on the microcapsule's morphology.

It was recently reported that PNIPAm−PEG−PNIPAm triblock copolymers in mixtures with PNIPAm homopolymers could be used as potential cell encapsulation materials for the pancreatic β-cell MIN6.[42] However, this copolymer was synthesized using an alkali-earth metal initiator system that forms a strong base and that may affect the buffer used for cell encapsulation. This situation could ultimately lead to high cytotoxicity.

Our novel approach utilizes PNIPAm hydrogels with a "microcapsule" morphology to encapsulate cells. In this Article, we describe the synthesis of multicore−shell PNIPAm-*co*-Am-*co*-PEGMa microcapsules with improved cell viability. We utilized a liquid−liquid dispersion technique in a system of three immiscible liquids to prepare PNIPAm-*co*-Am-*co*-PEGMa multicore−shell microcapsules. The core−shell morphology was developed in situ and was fixed by photopolymerization using a novel microarray technique.[27] The morphology was also confirmed experimentally using laser scanning confocal microscopy (LSCM) and theoretically by spreading coefficient calculations. As a proof-of-principle, the molecular weight and concentration of PEG were systematically varied to determine the effect of these parameters on microcapsule microstructure, cell encapsulation, and the cell viability of yeast cells.

Some advantages of our cell encapsulation device design include the use of materials with low cytotoxicity and the employment of a gentle encapsulation technique that uses an aqueous medium with no organic solvents to preserve cell integrity.[31]

2. EXPERIMENTAL SECTION

2.1. Materials. All chemicals used in this study were purchased from Sigma-Aldrich (Milwaukee, WI) unless otherwise noted and were used as-received without further purification. *N*-Isopropylacrylamide (NIPAm) and acrylamide (Am) were used as comonomers. *N*,*N*′-Methylene acrylamide was used as the cross-linker (MBAm). Polyethylene glycol monomethyl ether monomethacrylate (PEGMa) macromonomer with M_n of 300 and 1100 g/mol was used as comonomer. Silicone oil (DC710) was used as the core-oil. 2,2-Dimethoxy-2-phenylacetophenone (Irgacure

dx.doi.org/10.1021/la203030j |*Langmuir* XXXX, XXX, 000–000

Table 1. Chemical Components of PNIPAm-Based Hydrogels and Their Functions

chemical	function	properties rendered to microcapsule
N-isopropyl acrylamide (NIPAm)	monomer	temperature responsive (LCST)
acrylamide (Am)	comonomer 1	tailor LCST
polyethylene glycol monomethyl ether monomethacrylate (PEGMa)	comonomer 2	stealth property and biocompatibility
	M_n 300 g/mol (n = 4.5)	
	M_n 1100 g/mol (n = 22.7)	
methylenebis(acrylamide) (MBAm)	cross-linker	insolubility
2,2-dimethoxy-2-phenylacetophenone (Irgacure 651)	initiate polymerization	oil-soluble photoinitiator
anthraquinone-2-sulfonic acid, sodium salt monohydrate	initiate polymerization	water-soluble photoinitiator

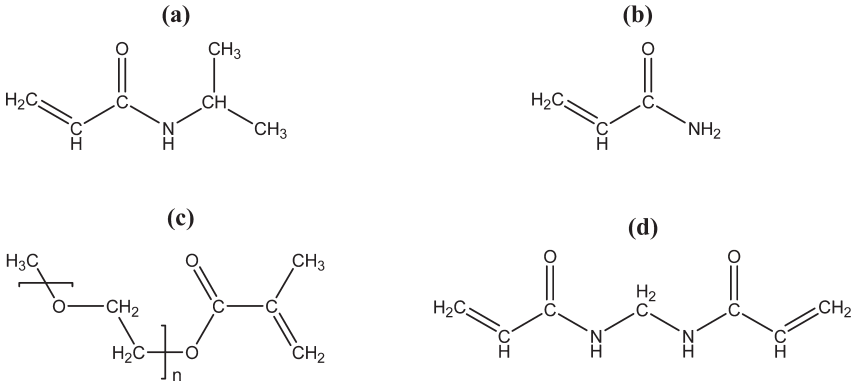

Figure 1. Chemical structures of monomers in aqueous solutions: (a) NIPAm, (b) Acrylamide, (c) PEG macromonomer, and (d) MBAm.

Scheme 1. Microarray Technique for Synthesis and Observation of Multicore−Shell Microcapsules

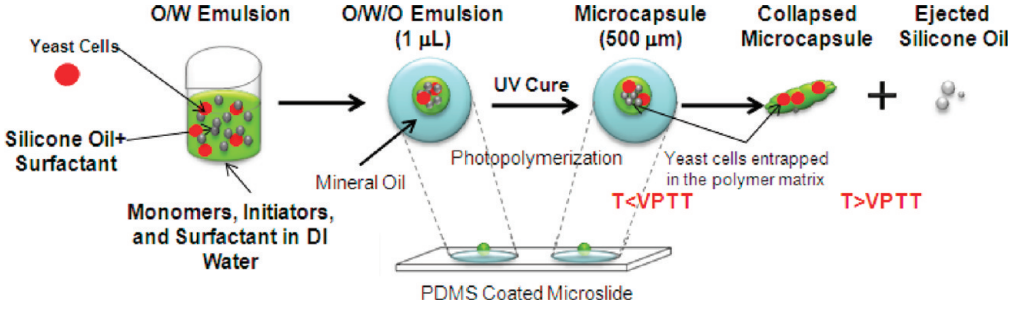

651) and anthraquinone-2-sulfonic acid, sodium salt monohydrate were used as oil-soluble and water-soluble photoinitiators, respectively. Fluorescein isothiocyanate (FITC) (Fluka) was used to fluorescently label the aqueous phase during the microcapsule synthesis and morphology study. Phosphate buffer saline (PBS) (GIBCO), *Saccharomyces cerevisiae* yeast (Baker's yeast), and a fluorescent viability probe for yeast, FUN1 (Invitrogen, NY), were used in the cell encapsulation and cell viability studies. Light density, medium viscosity mineral oil (Sigma Aldrich) was used as the continuous phase. Deionized (DI) water was purified using the Millipore Elix 3 system (18 MΩ cm resistivity) and was used in all experiments. A summary of the chemical compositions of PNIPAm-based hydrogels is shown in Table 1 along with their properties and functionalities. Chemical structures of NIPAm monomer and its comonomers are depicted in Figure 1.

2.2. Synthesis of PNIPAm-Based Microcapsules. NIPAm was copolymerized with Am and PEGMa. The molar ratio of NIPAm to Am is 95:5. For PEGMa macromonomer, the effects of various molecular weights (M_n = 300 and 1100 g/mol) and concentrations (10, 20, and 30 wt %) were investigated. A cross-linker MBAm in a molar ratio 1:750 (cross-linker/monomer) was added. These monomers were dissolved in DI water to make moderate solids content of 26 wt % total monomer concentration. In the present work, we used a simple microarray technique to synthesize microcapsules.[27] The microarray setup is illustrated in Scheme 1 and will only be briefly described here. Using PDMS (Sylgard 184)-coated hanging-drop microslides, we filled the cavities on the slide with 250 μL of mineral oil. Then aqueous (1 μL) droplets containing monomer, comonomers, cross-linker, photoinitiators, and fluorescent dye were placed on the surface of mineral oil in each microslide cavity. The photopolymerization was initiated by irradiating with UV light (Sylvania H44GS-100 Mercury Vapor Black Light) positioned 10 cm above the microslide. The polymerization was completed within 30−45 min with the final product a spherical hydrogel with a diameter of approximately 500 μm that floats on the surface of the mineral oil.

The synthesis of PNIPAm-based microcapsules with three immiscible liquids was accomplished using an emulsion of silicone oil-in-monomer solution. Silicone oil was vigorously mixed into the aqueous monomer

dx.doi.org/10.1021/la203030j |*Langmuir* XXXX, XXX, 000–000

solution to form an O/W primary (1°) emulsion. Surfactants comprised of 0.1 wt % Tween 80 and 1.5 wt % Span 80 were added to the aqueous phase and oil phase, respectively. These surfactants were used to stabilize the oil-in-water-in-oil (O/W/O) emulsion after the initial (O/W) was placed on the droplet of mineral oil. The photopolymerization was initiated as described before. In the case of the cell encapsulation studies, yeast cells were encapsulated into PNIPAm-based microcapsules by direct incorporation into the monomer solutions prior to photopolymerization.

The microcapsule in this study features multicore−shell morphology. Multiple microdomains of silicone oil form small compartments within the cross-linked polymer shell. This structure correlates with the theoretical morphology calculated by the spreading coefficient discussed later in the Results and Discussion.

2.3. Characterization. *2.3.1. Morphology of Microcapsules.* The morphology of the microcapsules was characterized using a laser scanning confocal microscope (LSCM) equipped with an argon (excitation at 488 nm) and a He−Ne (excitation at 543 nm) laser sources. The LSCM (Fluoview 300, Olympus) equipped with a digital camera (DP7, Olympus) allowed real-time observation of the hydrogels. Fluorescence dye, FITC, was added to the aqueous phase containing monomer droplets as they polymerized into hydrogel microspheres and eventually into microcapsules. Rhodamine B dye was added to silicone oil to observe its encapsulation into the inner structure of the microcapsules. The samples were observed under the LSCM, using two laser excitation sources (488 and 543 nm) and two acquisition channels at 518 and 580 nm, respectively, for FITC and Rhodamine B.

2.3.2. Cell Viability Experiment. LSCM was used in conjunction with a FUN1 fluorescence viability probe to determine the cell viability of yeast cells encapsulated in PNIPAm-based microcapsules. Yeast cells are excellent models of eukaryotic organisms and can be used to explore the lethal effects of various physical and chemical agents. A yeast cell suspension with a concentration of 10^6 cells/mL was prepared in PBS solution and incubated in a dark room at 37 °C for 24 h. The yeast cells were then mixed with 5 μM FUN1 dye by mild sonication to stain the cells. Microcapsules loaded with yeast cells were prepared by incorporating a mixture of FUN1-stained yeast cells in PBS into the monomer solutions. In this study, no fluorescence dye (FITC) was used in the polymer matrix or silicone oil phase. The microcapsules were then synthesized using the microarray technique as described in the previous section. The final concentration of monomers was maintained at 26.5 wt/v %. LSCM images were taken every 15 min during photopolymerization. Two settings on the LSCM were applied to acquire images of yeast cells with the microcapsules. First, a fluorescein long-pass filter set with excitation (λ_{ex}) at 485 nm and emission (λ_{em}) at 510 nm was used to observe the cell wall stained fluorescence green. Second, a filter allowing λ_{ex} 555 nm and λ_{em} 580 nm was used to observe the intravacuolar structures of metabolically active yeast cells labeled fluorescent red. In general, all cells will be stained and will fluoresce green at the cell wall, but only viable cells appear red due to the metabolic activity of a living cell as seen in Figures 2 and 3a. As a result, live and dead cells were distinguished. A control experiment was conducted with yeast cells in a warm solution of sucrose. Living cell samples were prepared from this solution by placing the solution on a glass slide and observing immediately with LSCM (Figure 2). A dead cell sample was prepared by heating a glass slide with the yeast cell solution to 80 °C for 2 min and then observed with LSCM as before (image not shown). The intensity of emitted light in fluorescence green was measured and translated into the number of total cells which exist in the area of interest. The number of spots that showed the intensity of fluorescence green represents all of the cells (Figure 3b), and the number of spots that showed the intensity of fluorescence red represents only the live cells (Figure 3c). The cell viability was then calculated using the following equation:

$$\text{cell viability } (\%) = (\text{number of live cells/number of total cells})*100 \quad (1)$$

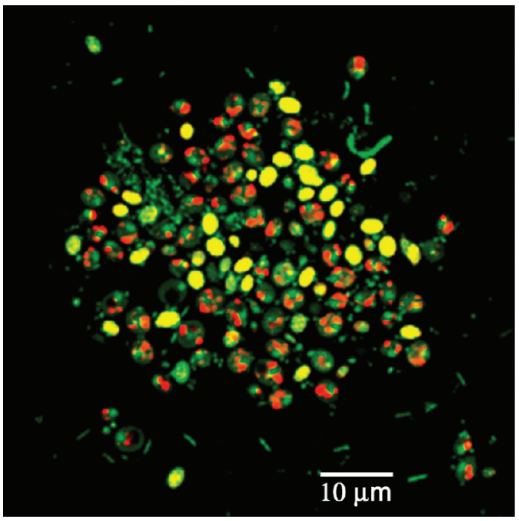

Figure 2. *Saccharomyces cerevisiae* yeast cells stained with FUN1 were viewed by LSCM. The cell wall of all stained yeast cells appears under the confocal microscope in florescence green (λ_{ex} 495 nm and λ_{em} 518 nm). Only the live cells, however, fluoresce red (λ_{ex} 555 nm and λ_{em} 580 nm) due to their metabolic activity.

3. THEORY

3.1. Relationship between the Interfacial Spreading Coefficient in Three Immiscible Liquids and Microcapsule Morphology. Pioneering work describing the various possible equilibrium morphologies adopted by three immiscible liquids was published previously by Torza and Mason.[43] They were able to predict the necessary conditions for microcapsule formation by various interfacial tensions between three immiscible liquid droplets, designated as phases 1, 2, and 3. The interfacial tensions between two liquids, for example (γ_{ij}), can be readily used to predict the resulting equilibrium morphology through spreading coefficients (S_i) for each phase as given by the general equation:

$$S_i = \gamma_{jk} - (\gamma_{ij} + \gamma_{ik}) \quad (2)$$

where the subscripts i, j, and k are for each liquid.

For the specific case of $\gamma_{12} > \gamma_{23}$ resulting in the $S_1 < 0$, Torza and Mason[43] proposed that there are only three possible combinations of S_i:

$$S_1 < 0;\ S_2 < 0;\ S_3 > 0 \quad (3)$$

$$S_1 < 0;\ S_2 < 0;\ S_3 < 0 \quad (4)$$

$$S_1 < 0;\ S_2 > 0;\ S_3 < 0 \quad (5)$$

The morphologies obtained when the conditions for each of the equations are satisfied are depicted schematically in Figure 4 and described as follows. When the conditions in eq 3 are satisfied, the particles adopt a core−shell morphology with a single (case A) or multiple inner-core (case B). When eq 4 is satisfied, "acorn"-shaped particles are formed (case C); and when eq 5 is satisfied, two separated droplets are preserved (case D).

The approach by Torza and Mason can be broadly applied to determine when the engulfing will occur in various encapsulation systems. Sundberg,[44] by applying Torza and Mason's approach, presented a thermodynamic analysis of the morphology of a system comprising a polymer encapsulating a relatively large-size

dx.doi.org/10.1021/la203030j |*Langmuir* XXXX, XXX, 000–000

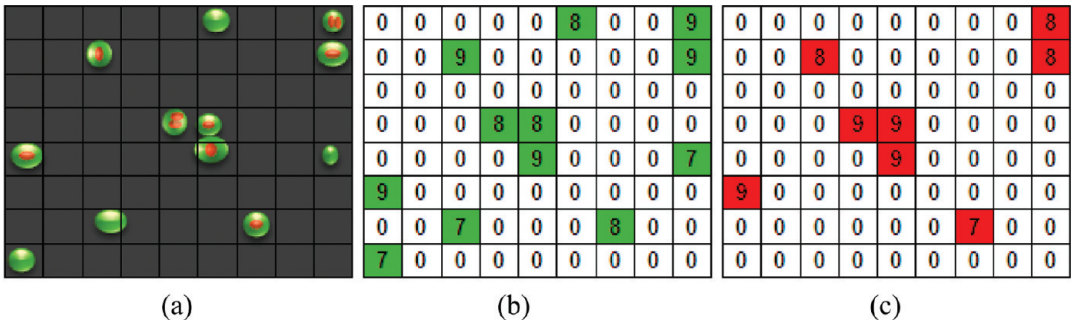

Figure 3. (a) Illustration of the process for live−dead cell counting using a fluorescence viability probe, FUN1. (b) The number of spots that fluoresce green represents all of the cells, and (c) the number of spots that fluoresce red represents only live cells.

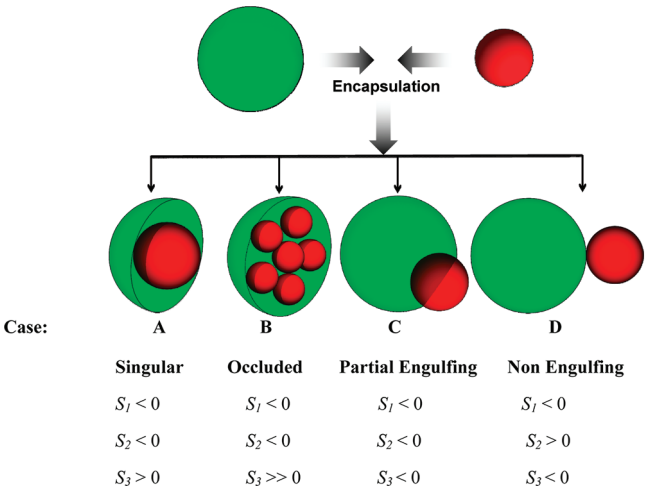

Figure 4. The possible morphologies for three immiscible liquids. The green and red represent two immiscible liquid droplets dispersed in a continuous phase (no color).

oil droplet in the micrometer range. Their analysis revealed that the interfacial tension of each phase is the key factor governing the type of microcapsules formed. Dimonie et al.[45] supported experimentally the hypothesis that, in addition to the viscosity of the monomers and oligomers (related to the chain mobility), the interfacial tension of the polymer phases is one of the main parameters controlling the particle morphology in a composite polymer latex system.

As Loxley and Vincent[46] demonstrated, to make microcapsules, it is important that the oil/water interfacial tension is not significantly reduced by the emulsion stabilizer. This restriction reduces the propensity for the oil/water interface to form.

These ideas were used in the present study to rationalize the particle morphologies observed. NIPAm, Am, MBAm, and PEGMa comonomers were used to form the polymer that phase separates within the emulsified droplets and subsequently encapsulates silicone oil into the inner core. Although in our case the shell polymer is eventually solid, and the oil is eventually removed leaving hollow cores, our analysis is still valid because on phase separation, the polymer is a water-rich liquid before it is cross-linked.

It is worth noting here that while Mason,[43] Atkins,[47] and others obtained single core−shell morphology when $S_1 < S_2 > S_3$, we obtained occluded structures (multicores, as shown in case B, Figure 4). The difference is probably due to the fact that occluded structures are more thermodynamically favorable than single occlusions for cross-linked systems.[48]

3.2. Calculations To Determine Interfacial Energy in Core−Shell PNIPAm Microcapsules. To predict whether a stable core−shell morphology will be formed for the current system, the spreading coefficients (S_1, S_2, and S_3) for each of the three phases can be determined using eq 2. To do this, first the interfacial energies between the three liquids (and eventually the polymer phase), that is, γ_{12}, γ_{23}, and γ_{13}, will be determined. This was accomplished in two steps as follows.

3.2.1. Determination of Interfacial Energy between PNIPAm and Oils (γ_{23} and γ_{13}). Phases 1, 2, and 3 correspond to the silicone oil phase (containing 1.5 wt % Span 80), mineral oil, and the aqueous phase (containing 0.1 wt % Tween 80 and comonomers), respectively. To determine the interfacial energies between PNIPAm−mineral oil and PNIPAm−silicone, that is, γ_{23} and γ_{13}, Young's equation can be used:

$$\gamma_{SL} + \gamma_{LV} \cdot \cos\theta = \gamma_{SV} \quad (6)$$

In eq 6, γ is the interfacial tension between two phases, and the subscripts S, L, and V represent solid, liquid, and vapor phases, respectively. Therefore, in regards to our system, γ_{23} and γ_{13} are γ_{SL} in Young's equation.

The interfacial or surface tensions (γ_{LV}) of the aqueous phase (containing 0.1 wt % Tween 80 and comonomers), mineral oil, and silicone oil (containing 1.5 wt % Span 80) were determined by the du Noüy ring method using a Lecomte du Noüy surface tensiometer (Krüss). The temperature was maintained at 22.5 °C (±0.5). Manual measurements were made by pulling the ring through the interface from underneath, recording the mean of three measurements for each liquid. Once the surface tensions of each liquid are known, the contact angle of these liquids with the dried PNIPAm film was then measured. The measurements were made using a Krüss Drop Shape Analyzer, DSA 100, by taking the mean contact angle of three measurements.

In regards to measurements of contact angles of the PNIPAm films, it is assumed that the planar film surface is representative of the microcapsule shell surface. This is because the recipe, time, and thus the temperature of polymerization using the UV lamp were kept the same as those for the droplets polymerized on the microslide. Contact angle measurements of the various liquids on PNIPAm films were conducted at T < VPTT because UV polymerization (when formation of the microcapsule's morphology occurs) was also conducted at T < VPTT.

To determine the interfacial or surface energy of PNIPAm film (γ_{SV}), we estimate it indirectly using the Zisman theory[49] (see

dx.doi.org/10.1021/la203030j |*Langmuir* XXXX, XXX, 000–000

the Supporting Information for details on the measurements and calculations).

3.2.2. Determination of Interfacial Energy between Silicone oil and Mineral Oil (γ_{12}). The interfacial tension between silicone oil and mineral oil (γ_{12}) cannot be obtained using Young's equation. Instead, the Young−Dupree equation was used:

$$\gamma_{12} = \gamma_1 + \gamma_2 - w_{12} \tag{7}$$

In eq 7, w_{12} is the pair potential energy, which characterizes the energy of interaction between two semi-infinite phases to give the interactions per unit area as shown in eq 8:

$$w_{12} = \frac{A_{12}}{12 \cdot \pi \cdot D_0^2} \tag{8}$$

where A_{12} is the Hamaker constant and D_0 is the characteristic cutoff or interaction distance. The Hamaker−Lifshitz theory is then used to estimate the Hamaker constant for the van der Waals interactions between the phases. This can be estimated from the dielectric polarizability (e.g., refractive index as a function of frequency and static dielectric constant) of the bulk phases. As shown by eq 9, the formula derived by Israelachvili[49] can be used for estimating the Hamaker constant (A), as an approximation when complete dielectric data are not available:

$$A_{ij} \approx \frac{3}{4} \cdot KT \cdot \left(\frac{\varepsilon_i - \varepsilon_a}{\varepsilon_i + \varepsilon_a}\right) \cdot \left(\frac{\varepsilon_j - \varepsilon_a}{\varepsilon_j + \varepsilon_a}\right) + \left(3h\nu_e \cdot \frac{(n_i^2 - n_a^2)(n_j^2 - n_a^2)}{8\sqrt{2} \cdot \sqrt{n_i^2 + n_a^2} \cdot \sqrt{n_j^2 + n_a^2} \cdot (\sqrt{n_i^2 + n_a^2} + \sqrt{n_j^2 + n_a^2})}\right) \tag{9}$$

In eq 9, K is Boltzmann's constant, T is the absolute temperature, ε is the zero frequency or static dielectric constant, h is Plank's constant, ν_e is the adsorption frequency in the ultraviolet, the main electronic absorption for the dielectric permittivity, and n_0 is the refractive index extrapolated to zero frequency. This formula assumes that the adsorption frequency is the same for all three phases. Phases 1 and 2 are the bulk phases representing the inner-core silicone oil and the continuous mineral oil phase, respectively, and phase 3 is the polymer phase. The second term of the sum is due to London-dispersion, van der Waals interactions. When the refractive index of phase 3 is intermediate between the values of phases 1 and 2, the London-dispersion term is negative. This condition favors the spreading of phase 3 between 1 and 2, that is, the formation of a core−shell microcapsule morphology.

The details of the Hamaker constant calculation are reported in the Results and Discussion.

4. RESULTS AND DISCUSSION

4.1. Microcapsule Morphology from Spreading Coefficient and Interfacial Energy Calculations. *4.1.1. Rationale for Spreading Coefficient Calculations Using Solid Polymer Film.* Initially, the surface tensions of the monomer solution (35 mN m^{-1}) were used to calculate the spreading coefficients. All spreading coefficients obtained (S_1, S_2, and S_3), however, were negative, predicting the thermodynamic equilibrium morphology to be partial engulfing or "acorn" morphology, which did not correlate to our experimental results. Dimonie et al.[45] found experimental evidence that, in addition to the viscosity of the monomers and oligomers (related to the chain mobility), the interfacial tension of the polymer phases is one of the main parameters controlling the particle morphology in a polymer latex system. We hypothesized that in our system there are two main factors influencing the experimentally obtained morphology. The first is the interfacial tension (surface energy) of the growing oligomer and polymer, and the second is the role of the aqueous phase surfactant (Tween 80) in partitioning between the phases to stabilize the 1° O/W emulsion formed by high-shear ultrasonication. The polymer chain motility and partitioning of the surfactant (as related to diffusion) and speed of the emulsion process (as related to reaction kinetics) need to be taken into account. Thus, the surface energy of the polymer phase was determined indirectly using Zisman theory and the interfacial tension between the 1° O/W emulsion is determined via contact angle measurements, and subsequent spreading coefficient calculations correctly predicted the experimentally obtained morphology once the polymer phase was accounted for as described in the following section.

4.1.2. PNIPAm Microcapsules. To evaluate the van der Waals attraction and to quantify the interfacial energy between phases, which is the driving force for encapsulation, the Hamaker constants (A) of silicone oil and mineral oil used in this study were calculated using eq 9. The spreading coefficients of the PNIPAm microcapsule system were calculated using the interfacial tension values obtained from the measurements of contact angles and surface tensions as described in the experimental and theoretical section. These parameters, as well as the pair potential energy (w), were calculated and are summarized in Table 2. The variables and parameter values used in the calculations are shown in Supporting Information Table S1.

Using eqs 6 and 7, the corresponding interfacial energies are calculated to be $\gamma_{12} = -2.88$ mJ m^{-2}, $\gamma_{31} = -2.27$ mJ m^{-2}, and $\gamma_{32} = 61.08$ mJ m^{-2}. The negative interfacial tension of the two oils on the PNIPAm solid surface indicates that the PNIPAm surface has a surface energy greater than the oils, and therefore the oils tend to spread over the solid surface to minimize the potential energy of the system. Moreover, the net negative interfacial tension gives rise to a thermodynamically unstable interface, which leads to spontaneous emulsification.

On the basis of these calculations, once the monomers are dispersed in the aqueous phase and then mixed via high-shear ultrasonication with silicone oil to generate the 1° oil/water emulsion, the Tween 80 and Span 80 preferentially adsorb at and partition between the water/oil interfaces so as to minimize the surface free energy of the system. Subsequently, the morphology is fixed after photopolymerization. As a result, the balance of interfacial energies should be as shown in equation:

$$\gamma_{12} > \gamma_{23} + \gamma_{13} \tag{10}$$

where 1 = silicone oil, 2 = mineral oil, and 3 = PNIPAm. Thus, due to the balance of surface activity achieved by the contribution of Tween 80 in the aqueous phase and Span 80 in the silicone oil phase, the aqueous monomer spreads over the surface of the silicone oil, and the core−shell morphology is spontaneously formed within the emulsion droplet to minimize its surface free energy.[34,35]

From the measured values of contact angle and surface tension, the calculated spreading coefficients of the liquids in the system are $S_1 = -61.7$ mN m^{-1}, $S_2 = -60.5$ mN m^{-1}, and $S_3 = 66.2$ mN m^{-1}. These values satisfied the condition that the

dx.doi.org/10.1021/la203030j |*Langmuir* XXXX, XXX, 000–000

microcapsule will adopt core−shell morphology ($S_1 < 0$; $S_2 < 0$; $S_3 < 0$). This result confirms the morphology of our PNIPAm microcapsule as shown in Figure 5.

Torza and Mason[43] applied eq 2 and the subsequent inequalities to a variety of low-molecular weight liquid (mostly hydrocarbons) dispersions in water and found agreement between their predictions and experimental results. It should be noted that they worked with incompatible pairs of low-viscosity liquids that diffuse rapidly and lead to the lowest interfacial energy morphology within the time frame of the experiment. By contrast, in the current study, at any given instant in time, once the UV light had initiated polymerization, the system is comprised of a complex dispersion of oils, water, monomer, monomer radicals, oligomers, oligomer radicals, and growing polymer chains. The latter would be amphiphilic in nature tending to partition to the various oil−water interfaces, decreasing their respective interfacial tensions, and then would eventually phase separate out of solution once their limit of water solubility had been reached as shown schematically in Figure 6.

To investigate the validity of the hypothesis that two factors, the presence of the polymer phase and the partitioning behavior of the aqueous phase surfactant, influence the droplet morphology in the current system, a series of experiments was conducted. In the experiments, summarized in Supporting Information Table S3 and Figures S3−6, systematic changes to the experimental parameters allowed the morphologies formed to be studied and characterized.

In our O/W/O double emulsion system, our polymers (PNIPAm and PNIPAm-*co*-PEGMa) are of relatively high molecular weight whose diffusional resistance may be such that the equilibrium morphology was not realized during the time frame of the experiment even though the driving force (thermodynamically driven to lower energies) continues to be present. Thus, Torza and Mason's work with low-viscosity liquids was a good way to test the correctness of the thermodynamic analysis, but it does not hold for high-molecular weight systems. As such, we have shown here that it is entirely possible to achieve nonequilibrium morphologies, especially in the case of emulsions, which are rate-limited and depend on the speed of the various processes (reaction kinetics and/or diffusion rates).

Table 2. Spreading Coefficients and Interfacial Tensions Calculated Separately for PNIPAm Microcapsule According to Equations 2−9

phase	liquid/substrate	spreading coefficient (mN m^{-1})
1	1.5 wt % Span 80 in silicone oil	$S_1 = -61.7$
2	mineral oil	$S_2 = -60.5$
3	PNIPAm polymer	$S_3 = 66.2$

interfacial tension (mN m^{-1})	interface	equation
$\gamma_{23} = \gamma_{SL} = -2.884$	mineral oil−PNIPAm	6
$\gamma_{12} = 61.076$	silicone oil−mineral oil	7
$\gamma_{13} = \gamma_{SL} = -2.2704$	silicone oil−PNIPAm	6

4.1.3. PNIPAm-co-PEGMa Microcapsules. For the PNIPAm-*co*-PEGMa copolymer system, the calculation of spreading coefficient was problematic. There was significant difficulty in measuring the contact angle of PNIPAm-*co*-PEGMa films with water or oil. Water completely spread and wet the copolymer film, which implied that PEG increased the wettability of the PNIPAm polymer. When measuring the contact angle of mineral oil or silicone oil, however, the oil also slowly spread over the PNIPAm-*co*-PEGMa film and ultimately wet the film as well, giving a final contact angle of 0. This result indicates two significant characteristics of the PNIPAm-*co*-PEGMa surface. First, PEG increased the surface hydrophilicity of the polymer film. Therefore, oils with lower surface tension will always spread and wet the higher surface tension surface. Second, PEG is well-known for possessing amphiphilic character and may act as a surfactant, thereby contributing to an increase of both the hydrophobic and the hydrophilic character of the PNIPAm-*co*-PEGMa films.

Subsequently, the contact angle of the PNIPAm-*co*-PEGMa films with water or oil could not be measured. The spreading coefficient of the system, however, can still be predicted. The contact angle results indicate that PEG increased the surface tension of the PNIPAm-*co*-PEGMa. This implies S_3 (polymer/aqueous phase) can only be increased. The silicone oil and mineral oil used in our system gave low surface tensions (31.8 and 29.6 mJ m^{-2}, respectively) and, therefore, yield negative spreading coefficients (S_1 and $S_2 < 0$), which satisfies the condition of an occluded multicore−shell morphology.

In summary, although formation of single-core and multicore−shell morphology requires a similar spreading condition, in the current system, that is, PNIPAm-*co*-PEGMa, only a multicore−shell morphology was obtained. The multiple-core microcapsule is believed to be a result of two factors: the high

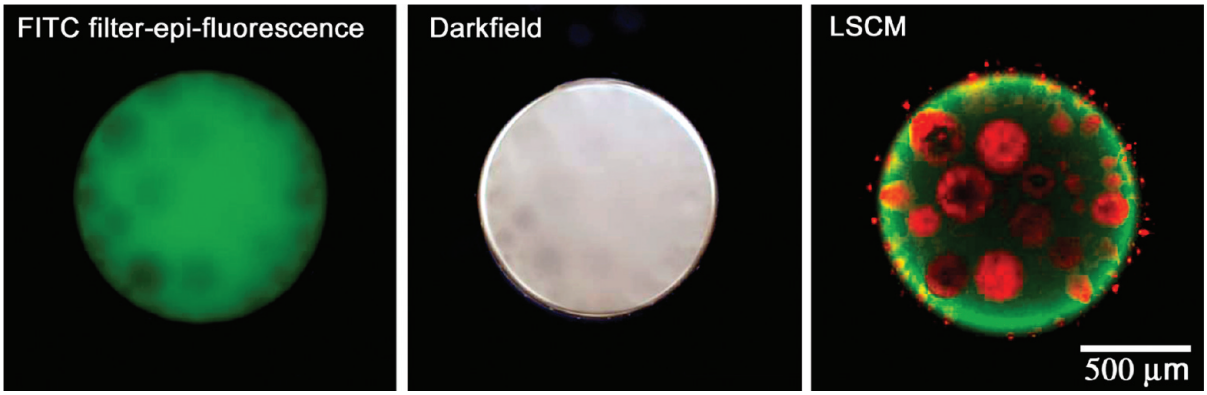

Figure 5. Representative confocal microscopy images of PNIPAm microcapsules (three liquid phases) showing the multicore−shell morphology. The microcapsules feature encapsulated silicone oil liquid forming multiple cores (fluorescence red) in a PNIPAm shell (fluorescence green). The continuous phase of mineral oil did not have any fluorescence dye and as such appears black.

dx.doi.org/10.1021/la203030j |*Langmuir* XXXX, XXX, 000–000

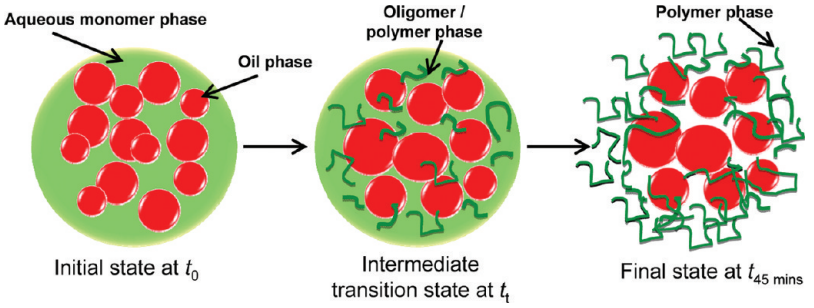

Figure 6. Schematic of the emulsion polymerization process in the oil-in-water-in-oil systems.

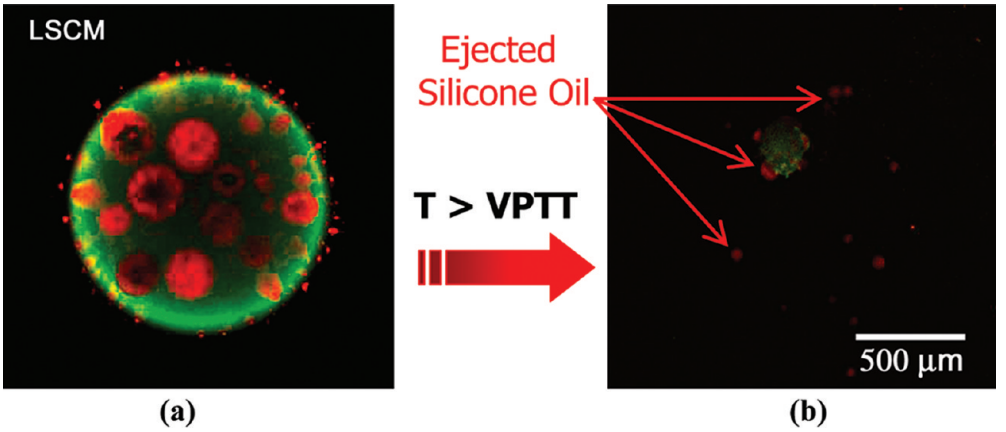

Figure 7. Confocal microscopy images of PNIPAm microcapsule using (a) LSCM at T (25 °C) < VPTT, and (b) LSCM at T (45 °C) > VPTT, demonstrating ejection of the inner core (silicone oil). An incomplete polymerization caused the microcapsule to rupture as it was deswollen. Oil-soluble initiator was used.

molecular weight polymers preventing diffusion of silicone oil to the mineral oil/water interface and the partitioning of the aqueous phase surfactant (Tween 80) to stabilize the 1° emulsion droplet. As explained earlier, a negative interfacial tension of silicone oil and PNIPAm is delineated to favor spontaneous emulsification due to a thermodynamically unstable interface. As a result, an emulsion of silicone oil was formed within the polymer aqueous phase, and this morphology was fixed as the photopolymerization took place at a faster rate than the diffusion of silicone oil to give the thermodynamically favored equilibrium acorn morphology.

4.2. Microcapsule Morphology by LSCM. A series of microcapsules were synthesized using the microarray technique as illustrated in Scheme 1. The actual process of microcapsule formation with the PNIPAm emulsion droplet was followed directly using the LSCM and the optical microscope. A series of images presented in Figure 5 show the change in appearance of a representative droplet under epi-fluorescence, dark-field, and LSCM modes. The equilibrium morphology of the microcapsule was a multicore−shell structure. The silicone oil (fluorescence red) was encapsulated within the PNIPAm polymer hydrogel (fluorescence green) as multiple cores. The fluorescence green is due to the excitation of FITC dye that was added to the monomer phase to enhance visualization of the outer shell once the microcapsule is formed, and the fluorescence red is due to Rhodamine B added to the silicone oil. This structure is in agreement with that predicted by our theoretical calculations of the spreading coefficient. A similar structure was also observed for aqueous core−shell particles reported by Atkins et al.[47] It should be noted that PNIPAm-*co*-PEGMa also formed multicore−shell structures, which can be seen in Figure 9.

4.3. PNIPAm-*co*-PEGMa Microcapsules: Temperature Response and the Loci of the Photoinitiators. Previously, we reported that PNIPAm-*co*-PEGMa functioned as a thermoresponsive hydrogel.[50] That is, PNIPAm-*co*-PEGMa microgels formed using two-liquid phases (W/O), having a thermoresponsive character with the transition temperature depending on the M_n of PEGMa. The deswelling behavior of the microgel shifted to higher temperatures and over a wider temperature range when PEG was incorporated into PNIPAm-*co*-Am. It was also found that the transition temperatures were sharper at lower PEG M_n and lower PEG concentrations.[50]

The effect of temperature on our PNIPAm-*co*-PEGMa microcapsules formed using three-liquid phases (O/W/O) was characterized in the current study. The ejection of silicone oil-inner core (dyed with Rhodamine B, red) as the temperature increased above VPTT is shown in Figure 7. The shell of PNIPAm collapsed and partially ruptured. This result was not expected as a chemically cross-linked hydrogel should remain intact during the deswelling process. Physical probing of this microcapsule indicated that this particle was only partially polymerized. It is important to note that this microcapsule was synthesized using only the oil-soluble photoinitiator, 2,2-dimethoxy-2-phenylacetophenone (Irgacure 651). This recipe worked well for synthesizing microgels (O/W) as reported previously.[50] Subsequent optimization of the polymerization time and recipe was conducted,

dx.doi.org/10.1021/la203030j |*Langmuir* XXXX, XXX, 000–000

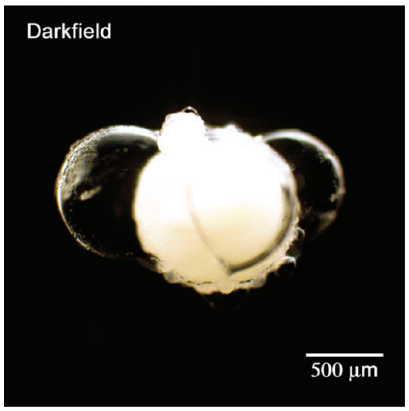

Figure 8. Dark field microscopy image of a representative PNIPAm microcapsule at T (45 °C) > VPTT. The thermal response was instantaneous at T > VPTT, and the fully cured microcapsule remained intact while the oil cores were ejected. Both oil-soluble and water-soluble photoinitiators were used.

and it was found that the addition of a water-soluble photoinitiator was required to completely polymerize the double emulsion (O/W/O).

One can hypothesize that the oil-soluble photoinitiator (2,2-dimethoxy-2-phenylacetophenone) partitioned to the interface between the silicone oil core and the aqueous phase containing monomers. Consequently, it became less available in the aqueous phase for photopolymerization of our water-soluble monomers. Replacing the oil-soluble photoinitiator with the water-soluble photoinitiator (anthraquinone-2-sulfonic acid, sodium salt monohydrate) did not yield complete polymerization either. In this case, it is speculated that because the water-soluble photoinitiator is highly reactive and decomposes to produce free-radicals more readily than that of the oil-soluble photoinitiator, at a comparable UV light exposure (wavelength and light intensity), it may lead to faster recombination of the reactive free-radicals, consequently preventing complete polymerization. Another plausible explanation is the loci of free radicals in the aqueous phase versus the oil phase. Initially, reaction of the free radical with the monomer in the aqueous phase can take place easily as the monomers are also located in the aqueous phase. As the polymerization proceeds, however, the oligomer-radicals grow in length and when they approach their limit of water solubility may partition at the oil—water interface, thereby leaving the site of polymerization (the aqueous phase in the case of only water-soluble initiators). This latter situation can also prevent the polymerization from proceeding to completion. Proving these hypotheses was beyond the scope of this study, where our goal here was to optimize the recipe to achieve a core—shell microcapsule from the three liquid phases in our (O/W/O) double emulsion system. Subsequently, using both the oil-soluble and the water-soluble photoinitiators proved to be more effective in enabling complete polymerization of the microcapsules within 45 min. It is important to note here that using two photoinitiators gave reproducible core ejection while maintaining the integrity of the microcapsules in comparison to when one photoinitiator was used alone as shown in Figure 8. The thermal response was instantaneous at T (45 °C) > VPTT, and the microcapsule remained intact while the oil-cores were ejected.

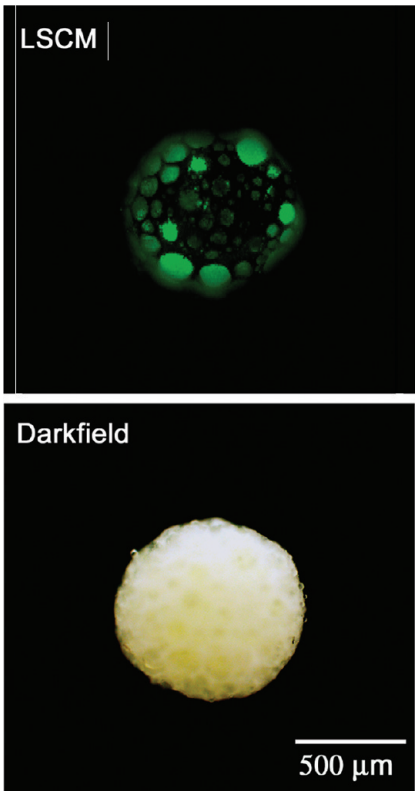

Figure 9. Representative confocal microscopy images of microcapsules comprised of 26 wt % PNIPAm-*co*-PEGMa (PEG M_n 300 g/mol) after polymerization and reswelling in an aqueous solution containing FITC dye showing that hollow compartments remain after silicone oil is ejected.

4.4. Hollow Microcapsules. The main role of the silicone oil is 2-fold. It facilitates multifunctionality in the microcapsule by first being used as a template to obtain the desired core—shell morphology, and second it can act as an encapsulant for oil-soluble drugs.

In the first mentioned case above, the silicone oil in the cores of the microcapsule can be released by heating the microcapsule to T > VPTT (Figure 8). The morphology of the microcapsule remained the same even after the silicone oil was ejected. Evidence of the hollow cores was obtained by reswelling the dried microcapsule in aqueous solution containing FITC dye to fill the "cores" as shown in Figure 9. Consequently, on the basis of these results, a multifunctional microcapsule can be designed as follows. A multicore microcapsule with biological cells embedded in the polymer matrix and silicone oil in the cores can be prepared. At T > VPTT, the silicone oil droplets can be expelled from the cores, leaving them hollow with the collapsed microcapsule intact. The microcapsules can then be reswollen with an aqueous solution containing a water-soluble drug that could be delivered in vivo by designing the VPTT to be close to physiological temperature. Using PEGylated microcapsules will prevent them from being detected by the body as a foreign agent, while the core of the microcapsule can be used to carry therapeutic agents or nutrients for the cells.

In the second case mentioned above, the oil cores can be used for delivery of oil-soluble drugs (e.g., doxorubicin, DOX). In such a case, the microcapsules are rendered multifunctional for cell encapsulation as well as for drug delivery. Immobilization of cells in the matrix of hydrogels has been previously reported,[32] but no

dx.doi.org/10.1021/la203030j |*Langmuir* XXXX, XXX, 000–000

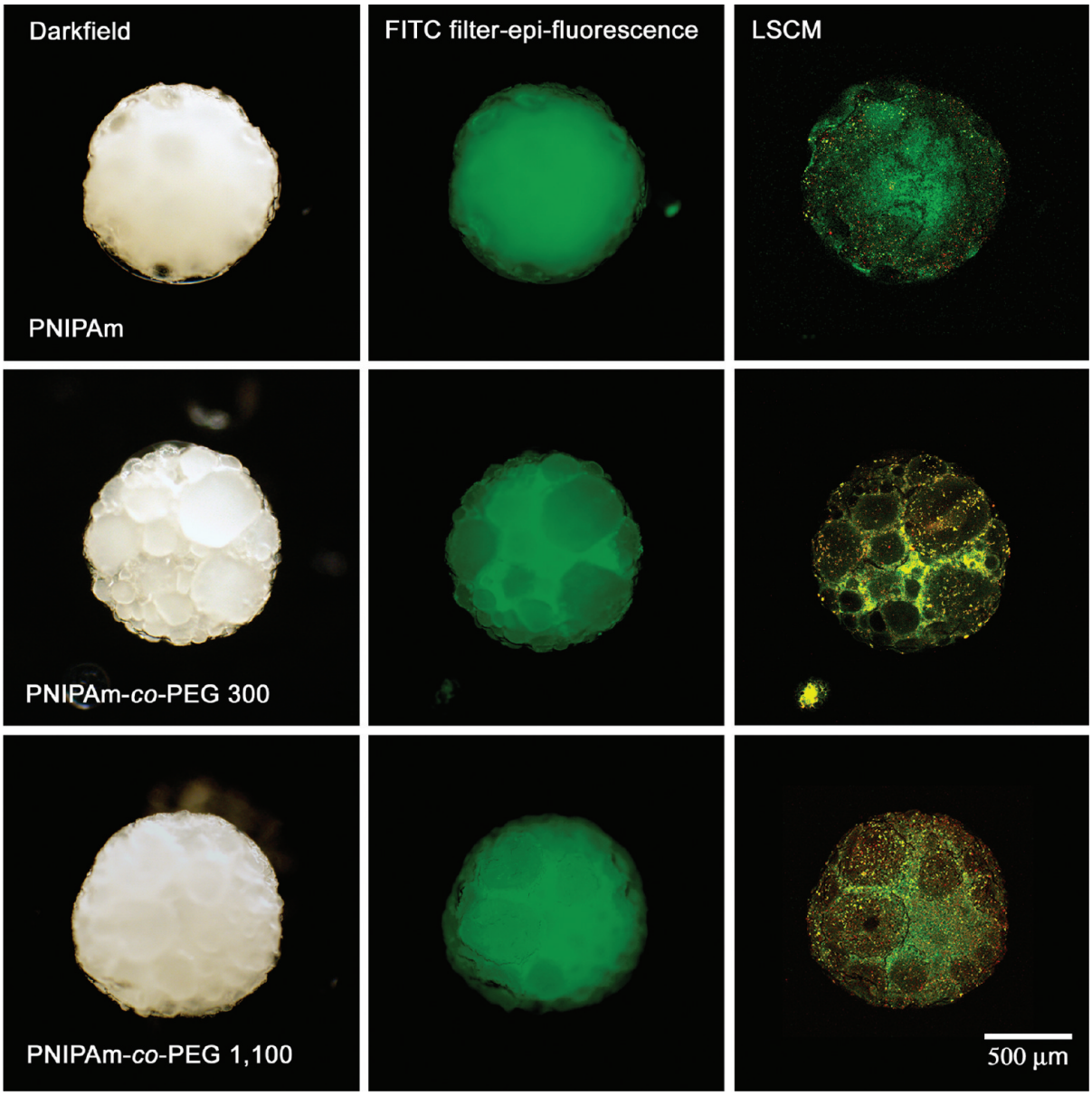

Figure 10. Representative confocal microscopy images of PNIPAm-based microcapsules containing encapsulated yeast cells after the polymerization was completed (UV irradiation time of 45 min). The images were taken at low magnification to reveal the morphology of the microcapsules and the distribution/location of the yeast cells in the polymer matrix. The FUN1 live/dead stain reveals that yeast cells both dead (fluoresce green) and alive (fluoresce red) were encapsulated and were also well dispersed within the polymer matrix.

study has reported hydrogels featuring a multicore morphology as described in the current study.

4.5. Cell Encapsulation. Yeast cells were chosen for this proof-of-principle experiment because they are fairly robust and can be easily seen by confocal microscopy. In the current study, (O/W/O) double emulsion-based microcapsules were investigated to encapsulate yeast cells. PNIPAm-*co*-PEGMa copolymer microcapsules for cell encapsulation were synthesized by mixing the monomer solution and a cell suspension prepared in phosphate-buffered saline solution, PBS, with a pH of 7.2. The cells were spontaneously encapsulated as the hydrogel formed. The distribution of cells depended on the polymer system. In the current system, the monomers are water-soluble, so they can be dissolved in various cell culture media. Confocal microscopy revealed that the encapsulated yeast cells were excluded from the silicone-oil cores and were found to be homogeneously distributed in the polymer matrix. It was also found that the yeast cells could not be ejected from the microcapsules as they remained entrapped in the polymer matrix at $T >$ VPTT.

4.6. Cell Viability of Yeast Cell Encapsulated in PNIPAm-Based Microcapsules. It was previously reported that protein adsorption (bovine serum albumin) significantly decreased as the degree of PEGylation increased in PNIPAm-based microgels. Specifically, the microgels became more biocompatible with increasing PEG content. A PEG content of 20 wt % was found to be sufficient to provide full surface coverage of the microgel, and thus a stealth effect was obtained.[50]

Cell viability is another measure of biocompatibility. The cell viability of yeast cells encapsulated within PNIPAm-based microcapsules was evaluated using a colorimetric technique. The yeast

dx.doi.org/10.1021/la203030j |*Langmuir* XXXX, XXX, 000–000

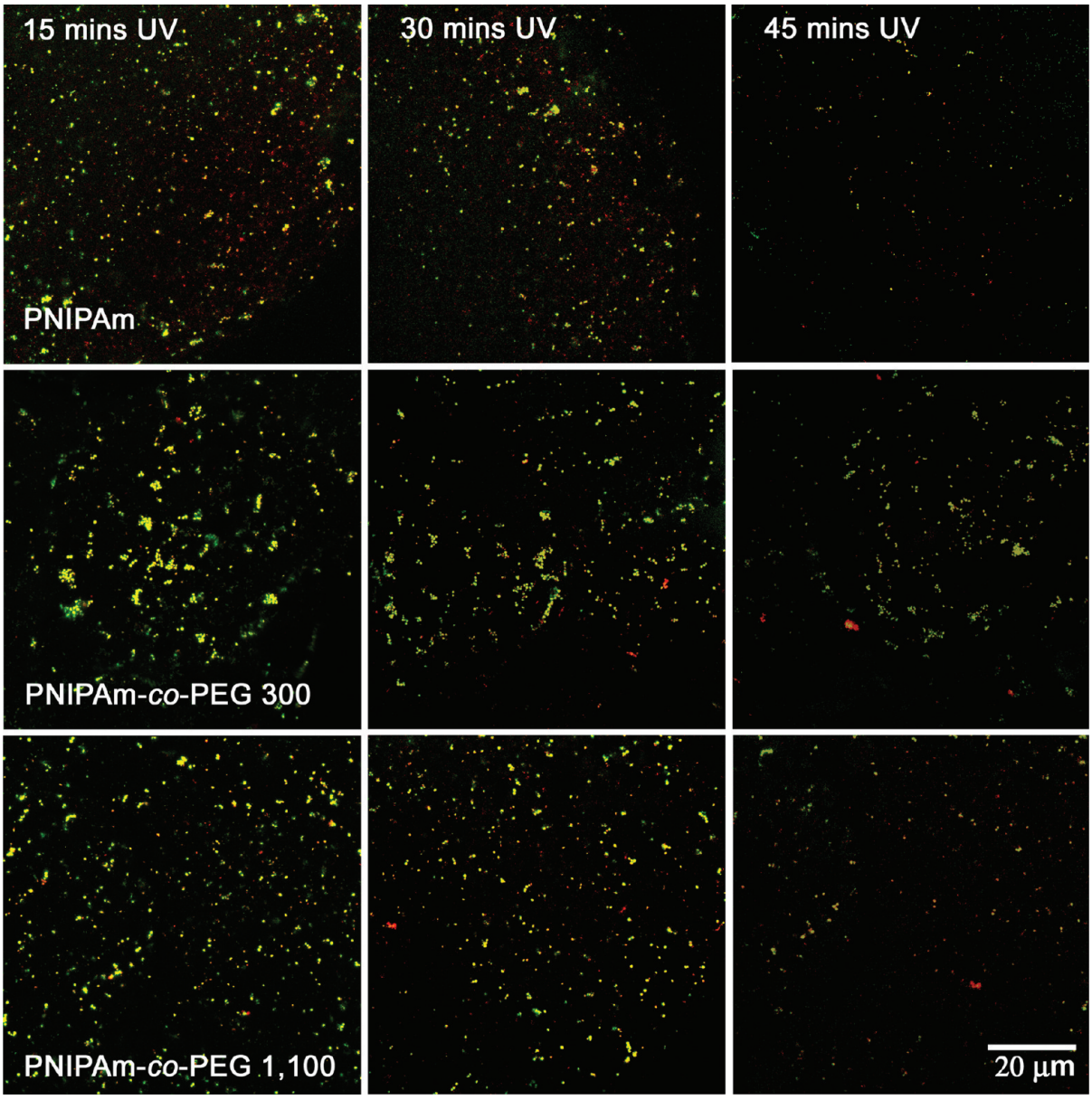

Figure 11. Representative confocal microscopy images of FUN1 live/dead stained yeast cells encapsulated in PNIPAm-based microcapsules. The images demonstrate the decrease of fluorescence intensity as a function of UV irradiation time. All images are 20× magnifications. The red signal visualizes the live cells.

cells were stained with only FUN1 dye and were observed under the LSCM microscope as shown in Figure 10. Using lasers that excite in the fluorescein and Rhodamine B ranges and their respective filters, a distinction between the live and dead cells can be made. In general, all stained yeast cells appear fluorescent green under the confocal microscope. Only the live cells, which are still metabolically active, are fluorescent red. The goal of the cell viability study was to monitor the rate of survival of the yeast cells during photopolymerization as well as after the polymerization was completed (UV irradiation time of 45 min). The yeast cells were directly encapsulated into the PNIPAm-based microcapsules by incorporating them into monomers prior to photopolymerization. Representative confocal images of microcapsules loaded with cells stained with FUN1 dye are shown in Figure 10. Yeast cells were observed in the aqueous phase (polymer matrix) but were not found in the silicone oil microdomains or outside the microcapsule in the mineral oil. That is, the cells formed small aggregates with strong red fluorescence observed inside the capsule, demonstrating high viability of yeast cells postencapsulation.

The change in intensity of FUN1 stained yeast cells as a function of UV irradiation is shown in Figure 11. As the UV irradiation time increased, the intensity of the stained yeast cells decreased, indicating that the health of the encapsulated yeast cells deteriorated with increasing time/dose of UV exposure. Some of the fluorescence red disappeared with increasing UV exposure. The number of yeast cells was then counted. The populations of the yeast cells with and without red fluorescence were distinguished to determine the cell viability of encapsulated yeast cells in each of the microcapsules.

dx.doi.org/10.1021/la203030j |*Langmuir* XXXX, XXX, 000–000

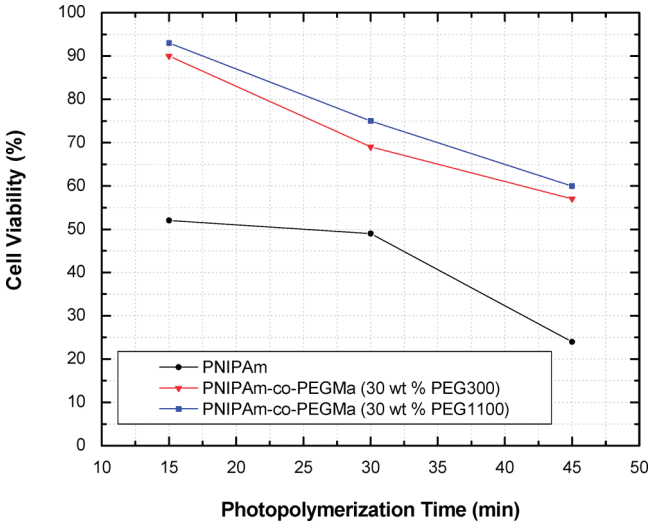

Figure 12. Comparison of cell viability (%) of yeast cells encapsulated within PNIPAm-based microcapsules and that using 30 wt % PEGMa M_n 300 and 1100 g/mol, respectively, as a function of UV irradiation time.

A comparison of the cell viability over the course of UV irradiation for the yeast cells encapsulated with PNIPAm, PNIPAm-*co*-PEGMa (30 wt % PEG M_n 300 g/mol), and PNIPAm-*co*-PEGMa (30 wt % PEG M_n 1100 g/mol) microcapsules, respectively, is shown in Figure 12. In general, the viability of yeast cells encapsulated in all microcapsules decreased as the UV irradiation time increased. Significantly low cell viability, however, of about 50% was observed in the case of PNIPAm microcapsules after a short period (15 min) of UV irradiation. This cell viability value is also significantly lower than that of the PEG modified PNIPAm microcapsules. This result indicates that the toxicity of the employed monomers is the dominant factor rather than the time/dose of UV irradiation. The high cytotoxicity of NIPAm monomer in contact with cells has also been reported by Vihola et al.[51] Cell damage was found to be dependent on the monomer concentration, temperature, and incubation time. The presence of PEG macromonomer in the monomer solutions in the present study, however, provides a positive effect in increasing viability of the encapsulated yeast cells. After 15 min of UV irradiation, a cell viability of 90% and 92% was achieved when 30 wt % PEG with M_n of 300 and 1100 g/mol, respectively, was incorporated. This benefit was obtained due to the lack of toxicity of PEG macromonomer as described earlier. The presence of PEG also reduces the chance of cells to come into direct contact with NIPAm monomer by diluting the NIPAm concentration. This results in a higher percentage of live cells in PNIPAm-*co*-PEGMa microcapsules.

In the study conducted by Vihola et al.,[51] they also reported that cytotoxicity of PNIPAm decreases as its molecular weight increases. In our system, however, as the polymerization proceeds (to 30 and 45 min photopolymerization) and the amount of monomers in the system decreases, we continued to observe cell death. The decline in cell viability as the photopolymerization time increased may be due to many factors including the presence of unpolymerized NIPAm monomer, the time of cell exposure to NIPAm monomer, the generation of free-radicals from UV radiation that lead to oxidation of the cell wall, heat from the UV lamp, as well as the lack of nutrition.

It should be noted that the PNPAm-based microgels and microcapsules were believed to be completely photopolymerized after 30 min of UV irradiation. For comparison, however, irradiation was continued for 45 min as the copolymerization of PNIPAm with PEG macromonomer increases the polymerization time. Longer polymerization time is required due to the increased probability of a long polyethylene oxide chain shielding the functional amine end group.[17] At the end of 45 min UV irradiation, as expected, the cell viability of the microcapsules of PEG modified PNIPAm is significantly higher (~60%) than that of PNIPAm (~25%). This result confirms that incorporating PEG increases cell viability of encapsulated yeast cells. A practical comparison is to compare cell viability at the end of polymerization. As such, cell viability in the PNIPAm microcapsule after 30 min of UV irradiation was 49%, and about 10% less than that of PEG modified PNIPAm microcapsules after 45 min UV irradiation.

It was also observed that there is an effect of M_n of PEG macromonomer on the cell viability. Microcapsules synthesized with larger PEG macromonomers (M_n 1100 g/mol) provided a slightly higher cell viability of 3−6% as compared to the smaller PEG macromonomer (M_n 300 g/mol). It is speculated that this may be due to the fact that the larger macromonomer of PEG possesses a higher number of oxygen atoms, providing a better hydration shell to prevent the cells from direct contact with the NIPAm monomer.

In summary, incorporating PEG into PNIPAm microcapsules is an effective way to improve the cell viability of yeast cells, which were loaded into PNIPAm-based multicore−shell microcapsules. The benefit of incorporating PEG into the system can be observed throughout the polymerization process from the beginning until the end.

5. CONCLUSIONS

This Article describes a simple yet effective method for living cell encapsulation using thermoresponsive multicore−shell PNIPAm-*co*-PEGMa microcapsules. Spreading coefficient calculations were found to correctly predict the core−shell morphology of the resulting microcapsules. Thus, an understanding of the relationship of interfacial tensions between the three liquid phases in the system is useful for designing microcapsules with the desired morphology and functionality. The cell viability improves significantly with PEGylation from the beginning of polymerization until the end. Low cytoxicity of the PNIPAm-*co*-PEGMa microcapsules demonstrates that these polymer networks are safe substrates for cell encapsulation and other tissue engineering applications.

■ ASSOCIATED CONTENT

Supporting Information. Tables and figures showing contact angle measurements for determining the critical surface tension according to Zisman theory. Results for the control experiments to validate the hypothesis that the interfacial tensions of the polymer phase and aqueous phase surfactant in the 1° emulsion influence the final morphology. This material is available free of charge via the Internet at http://pubs.acs.org.

■ AUTHOR INFORMATION

Corresponding Author

*E-mail: bridgette_budhlall@uml.edu.

dx.doi.org/10.1021/la203030j |*Langmuir* XXXX, XXX, 000–000

■ ACKNOWLEDGMENT

This work was financially supported by the University of Massachusetts, Lowell, new faculty startup funds and by the Massachusetts Technology Collaborative's John Adams Innovation Fund and the National Science Foundation, NSF (Award: ECE 0425826). T.T. also acknowledges the Government of Thailand for a National Scholarship.

■ REFERENCES

(1) (a) Chang, T. M. S. *Science* **1964**, *146*, 524. (b) Chick, W. L.; Like, A. A.; Lauris, V. *Science* **1975**, *187*, 847. (c) Lim, F.; Sun, A. M. *Science* **1980**, *210*, 908.

(2) Uludag, H.; De Vos, P.; Tresco, P. A. *Adv. Drug Delivery Rev.* **2000**, *42*, 29.

(3) Germain, M.; Balaguer, P.; Nicolas, J. C.; Lopez, F.; Esteve, J. P.; Sukhorukov, G. B.; Winterhalter, M.; Richard-Foy, H.; Fournier, D. *Biosens. Bioelectron.* **2006**, *21*, 1566.

(4) (a) Anal, A. K.; Singh, H. *Trends Food Sci. Technol.* **2007**, *18*, 240. (b) Kailasapathy, K. *Curr. Issues Intest. Microbiol.* **2002**, *3*, 39.

(5) Rabanel, J.-M.; Banquy, X.; Zouaoui, H.; Mokhtar, M.; Hildgen, P. *Biotechnol. Prog.* **2009**, *25*, 946.

(6) Ratner, B. D. In *Comprehensive Polymer Science*; Allem, G., Bevingtom, J. C., Eds.; Pergamon Press: Oxford, 1989; Vol. 7, p 201.

(7) (a) Hoffman, A. S. *Adv. Drug Delivery Rev.* **2002**, *54*, 3. (b) Saki, S.; Kawakami, K. *J. Biomed. Mater. Res., Part A* **2008**, *85*, 345.

(8) (a) Soon-Shiong, P. *Adv. Drug Delivery Rev.* **1999**, *35*, 259. (b) Soon-Shiong, P.; Heintz, R. E.; Merideth, N.; Yao, Q. X.; Yao, Z.; Zheng, T.; Murphy, M.; Moloney, M. K.; Schmehl, M.; Harris, M. *Lancet* **1994**, *343*, 950.

(9) Dong, L.; Hoffman, A. S. *J. Controlled Release* **1991**, *15*, 141.

(10) (a) Yamada, N.; Okano, T.; Sakai, H.; Karikusa, F.; Sawasaki, Y.; Sakurai, Y. *Makromol. Chem. Rapid Commun.* **1990**, *11*, 571. (b) Takezawa, T.; Mori, Y.; Yoshizato, K. *Bio/Technology* **1990**, *8*, 854.

(11) Kazakov, S. V. In *Smart Polymers: Application in Biotechnology and Biomedicine*; Mattiasson, I. C. a. B., Ed.; CRC Press: FL, 2002; p 8.

(12) Qu, T.; Wang, A.; Yuan, J.; Shi, J.; Gao, Q. *Colloids Surf., B* **2009**, *72*, 94.

(13) Wei, H.; Cheng, S. X.; Zhang, X. Z.; Zhuo, R. X. *Prog. Polym. Sci.* **2009**, *34*, 893.

(14) Yoshimura, H. *J. Chem. Phys.* **1984**, *81*, 6379.

(15) Heskins, M.; Guillet, J. E. *J. Macromol. Sci., Chem.* **1968**, *2*, 1441.

(16) Winnik, F. M. *Macromolecules* **1989**, *23*, 233–243.

(17) Pelton, R. *Adv. Colloid Interface Sci.* **2000**, *85*, 1.

(18) Schild, H. G. *Prog. Polym. Sci.* **1992**, *17*, 163.

(19) Sun, S. T.; Nishio, I.; Swislow, G.; Tanaka, T. *J. Chem. Phys.* **1980**, *73*, 5970.

(20) Pelton, R. H.; Pelton, H. M.; Morfesis, A.; Rowell, R. L. *Langmuir* **1989**, *5*, 816.

(21) Kim, K. H.; Kim, J.; Jo, W. H. *Polymer* **2005**, *46*, 2836.

(22) Schwall, C.; Banerjee, I. *Materials* **2009**, *2*, 577.

(23) Gan, D.; Lyon, L. A. *Macromolecules* **2002**, *35*, 9634.

(24) Nolan, C. M.; Reyes, C. D.; Debord, J. D.; Garcia, A. J.; Lyon, L. A. *Biomacromolecules* **2005**, *6*, 2032.

(25) Franzesi, G. T.; Ni, B.; Ling, Y.; Khademhosseini, A. *J. Am. Chem. Soc.* **2006**, *128*, 15064.

(26) Huo, D.; Li, Y.; Qian, Q.; Kobayashi, T. *Colloids Surf., B* **2006**, *50*, 36.

(27) Budhlall, B. M.; Marquez, M.; Velev, O. D. *Langmuir* **2008**, *24*, 11959.

(28) Wu, X.; Pelton, R. H.; Hamielec, A. E.; Woods, D. R.; McPhee, W. *Colloid Polym. Sci.* **1994**, *272*, 467.

(29) Guan, Y.; Zhang, Y. *Soft Matter* **2011**, *7*, 6375–6384.

(30) Nash, M. E.; Carroll, W. M.; Nikoloskya, N.; Yang, R.; Connell, C. O.; Gorelov, A. V.; Dockery, P.; Liptrot, C.; Lyng, F. M.; Garcia, A.; Rochev, Y. A. *ACS Appl. Mater. Interfaces* **2011**, *3*, 1980.

(31) Zhai, G.-Q.; Ying, L.; Kang, E. T.; Neoh, K. G. *Surf. Interface Anal.* **2004**, *36*, 1048.

(32) Kessler, D.; Théato, P. *Macromol. Symp.* **2007**, *249−250*, 424.

(33) Cole, M. A.; Jasieniak, M.; Voelcker, N. H.; Thissen, H.; Griesser, H. J. *Eur. Cells Mater.* **2007**, *14*, 50.

(34) Rockwood, D. N.; Chase, D. B.; Akins, R. E., Jr.; Rabolt, J. F. *Polymer* **2008**, *49*, 4025.

(35) Azarbayjani, A. F.; Venugopal, J. R.; Ramakrishna, S.; Lim, P. F. C.; Chan, Y. W.; Chan, S. Y. *J. Pharm. Pharm. Sci.* **2010**, *13*, 400–410.

(36) Šňupárek, J. *Acta Polym.* **1981**, *32*, 368.

(37) Gewehr, M.; Nakamura, K.; Ise, N.; Kitano, H. *Makromol. Chem.* **1992**, *193*, 249.

(38) Stoychev, G.; Puretsky, N.; Ionov, L. *Soft Matter* **2011**, *7*, 3277.

(39) Luo, D.; Pullela, S. R.; Marquez, M.; Cheng, Z. *Biomicrofluidics* **2007**, *1*, 034102.

(40) (a) Veronese, F. M.; Pasut, G. *Drug Discovery Today* **2005**, *10*, 1451. (b) Veronese, F. M. *Biomaterials* **2001**, *22*, 405. (c) Harris, J. M.; Chess, R. B. *Nat. Rev. Drug Discovery* **2003**, *2*, 214.

(41) Orive, G.; Hernandez, R. M.; Gascon, A. R.; Calafiore, R.; Chang, T. M. S.; Vos, P. D.; Hortelano, G.; Hunkeler, D.; Lacik, I.; Shapiro, A. M. J.; Pedraz, J. L. *Nat. Med.* **2003**, *9*, 104.

(42) Lu, H. F.; Targonsky, E. D.; Wheeler, M. B.; Cheng, Y. L. *Biotechnol. Bioeng.* **2007**, *96*, 146.

(43) Torza, S.; Mason, S. G. *J. Colloid Interface Sci.* **1970**, *33*, 67.

(44) Sundberg, D. C.; Casassa, A. P.; Pantazopoulos, J.; Muscato, M. R.; Kronberg, B.; Berg, J. *J. Appl. Polym. Sci.* **1990**, *41*, 1425.

(45) Dimonie, V. L.; El-Aasser, M. S.; Vanderhoff, J. W. *Polym. Mater. Sci. Eng.* **1988**, *58*, 821.

(46) Loxley, A.; Vincent, B. *J. Colloid Interface Sci.* **1998**, *208*, 49.

(47) Atkins, R.; Davies, P.; Hardy, J.; Vincent, B. *Macromolecules* **2004**, *37*, 7979–7985.

(48) Durant, Y. G.; Sundberg, D. C. *Macromolecules* **1996**, *29*, 8466.

(49) Israelachvili, J. N. *Intermolecular and Surface Force*, 2nd ed.; Academic Press, Elsevier Ltd.: MA, 2003; p 184.

(50) Trongsatitkul, T.; Budhlall, B. M. *Biomacromolecules* **2011**, in press.

(51) Vihola, H.; Laukkanen, A.; Valtola, L.; Tenhu, H.; Hirvonen, J. *Biomaterials* **2005**, *26*, 3055.